

Low-spin Mn^{3+} ion in rhombohedral $LiMnO_2$ predicted by first-principles calculations

Zu-Fei Huang, Fei Du, Chun-Zhong Wang, Deng-Pan Wang, and Gang Chen*

Department of Materials Science, College of Materials Science and Engineering, Jilin University, Changchun 130012, People's Republic of China

(Received 31 August 2006; revised manuscript received 28 November 2006; published 15 February 2007)

By means of first-principles calculations using spin-polarized generalized gradient approximation method, the Mn^{3+} ion in hypothetical rhombohedral $LiMnO_2$ (r - $LiMnO_2$) is predicted to be in an unusual low-spin state, i.e., all of its four $3d$ electrons occupy the three t_{2g} levels, which makes r - $LiMnO_2$ not only a good cathode material for rechargeable lithium-ion battery, but also a possible half-metal for spintronics. Following the proposed synthesis approaches deduced from the calculations, well crystallized r - $LiMn_{0.65}Cr_{0.35}O_2$ is obtained through hydrothermal reaction and the low-spin state of the Mn^{3+} ion is verified by magnetic measurements.

DOI: 10.1103/PhysRevB.75.054411

PACS number(s): 75.50.-y, 71.15.Nc, 71.20.-b, 75.30.Cr

I. INTRODUCTION

Encouraged by the success of layered rhombohedral $LiCoO_2$ (space group $R\bar{3}m$, hereafter denoted as r - $LiCoO_2$) applied as cathode in commercial rechargeable lithium batteries, enormous and extensive studies have been carried out on isostructural r - $LiMO_2$ ($M=3d$ transition metal) and their doped forms since last decade.¹⁻⁷ In this structure, the O^{2-} ions sublattice is face centered cubic and provides a framework where the Li^+ and M^{3+} ions occupy all the octahedral interstices, leading to fully separate and alternate two-dimensional triangular layers stacked with a sequence as M-O-Li-O-M (α - $NaFeO_2$ -type).³⁻⁵ Such a layered structure ensures the easy extraction/insertion of Li^+ ions upon the charge/discharge cycling. Because of its high theoretical capacity, nontoxicity and inexpensive Mn mineral, r - $LiMnO_2$ arouses special attention among r - $LiMO_2$.¹⁻⁷ However, under equilibrium conditions, pure $LiMnO_2$ is crystallized in a nonlayered orthorhombic structure ($Pm\bar{m}n$, o - $LiMnO_2$) where Li^+ as well as Mn^{3+} and O^{2-} ions are not located in their own individual planes.⁴ Such a structure makes Li^+ migration more difficult during the charge/discharge cycles and exhibits poor electrochemical activity.²⁻⁴

Layered monoclinic $LiMnO_2$ ($C2/m$, m - $LiMnO_2$), the Jahn-Teller (JT) distorted phase of r - $LiMnO_2$, was first synthesized *via* an ion exchange route from m - $NaMnO_2$ in 1996.^{1,2} Nevertheless, during electrochemical cycling m - $LiMnO_2$ converts irreversibly to a spinel-like structure, which results in remarkable capacity fading.^{4,5} It is believed that such a disadvantage is attributed to the wide and discontinuous variation in the magnitude of the cooperative JT effect during the redox cycles which accompany the Li^+ extraction/intercalation.^{4,5} Efforts of doping with other metal elements such as Co,⁵ Ni,⁶ and Cr (Ref. 7) thus have been conducted to suppress the cooperative JT distortion and stabilize the $C2/m$, even $R\bar{3}m$ symmetry. However, the understanding on the structural phase behavior of r - $LiMn_xM_{1-x}O_2$ ($M=Co$, Ni , and Cr) are somewhat inconsistent.^{4,5}

It is well known that in an octahedral complex, the five d orbitals of M ion are split into a set of lower threefold degenerate t_{2g} states and upper twofold degenerate e_g states by

the ligand field.³ Therefore, Mn^{3+} (d^4) ion in hypothetical r - $LiMnO_2$ can adopt three possible spin configurations, i.e., high-spin (HS, $t_{2g}^3e_g^1$, $S=2$), low-spin (LS, $t_{2g}^4e_g^0$ and occupying all three t_{2g} levels, $S=1$) and nonspin (NS, $t_{2g}^4e_g^0$ but occupying two of the three t_{2g} levels, $S=0$) states. Since the distortion from $R\bar{3}m$ symmetry and the structural instability of m - $LiMnO_2$ result from the JT active HS Mn^{3+} ion, it is reasonable to suppose that the Mn^{3+} ion in pure r - $LiMnO_2$ may be in the JT inactive, i.e., LS or NS states. However, to our knowledge, the synthesis of pure r - $LiMnO_2$ still remains a great challenge and purely an imaginative figment to materials scientists until now.

In the present work, we conduct first-principles calculations to investigate the electronic structures of r - $LiMnO_2$ with the three possible spin configurations, i.e., HS, LS, and NS states, and hope to suggest approaches for synthesizing r - $LiMnO_2$. The Mn^{3+} ion in this material is calculated to be in an unusual low-spin state, which is confirmed by the results of magnetic measurement on Cr-doped r - $LiMnO_2$.

II. PROCEDURES OF CALCULATION

All the calculations were carried out with the CASTEP package by plane-wave pseudopotential method.⁸ Since some previous studies have revealed that generalized gradient approximation (GGA) achieves greater accuracy for Mn-oxides compared to local density approximation (LDA) due to the enhanced localization and inhomogeneity integrated in GGA,^{9,10} we employed spin-polarized GGA (GGS) for the exchange-correlation potential. HS, LS, and NS states were simulated respectively by fixing the number of the unpaired electrons in the primitive cell as 4, 2, and 0. First, the structures of the primitive cells containing one r - $LiMnO_2$ formula unit were fully relaxed until the self-consistent field (SCF) convergence per atom, tolerances for total energy, root-mean-square (RMS) displacement of atoms, RMS force on atoms and RMS stress tensor are less than 2×10^{-6} eV, 2×10^{-5} eV, 0.001 Å, 0.05 eV/Å, and 0.1 GPa, respectively. Then the optimized structures were used to calculate the total energies and the electronic structures. An energy cutoff of 400 eV with a k mesh parameters $8 \times 8 \times 8$ was adopted.

TABLE I. The calculated spin of each Mn ions (S), relative total energies (ΔE) and cell volumes (V) per formula unit, optimized cell parameters (a and c), Mn-O bond lengths (L) of r -LiMnO₂ under the three possible spin states together with the experimental data of r -LiMn_{0.65}Cr_{0.35}O₂.

States	S	ΔE (meV)	V (Å ³)	a (Å)	c (Å)	L (Å)
HS	1.90	0	38.409	3.005	14.739	2.067
LS	1.00	11	34.630	2.866	14.600	2.002
NS	0.00	688	33.703	2.841	14.466	1.992
Exp.	1.07	-	32.579	2.801	14.386	-

III. RESULTS AND DISCUSSION

A. Spin state of Mn ion in r -LiMnO₂

As proven by the S value listed in Table I, the three possible spin states have been reproduced successfully. In the viewpoint of energy, the NS state is unstable with energy of 688 meV/f.u. higher than the HS state, the most stable solution among the three possible spin states. Apparently, the high-spin state should be the ground state of r -LiMnO₂. However, the LS state has comparable stability to the HS state with a higher energy of only 11 meV/f.u. Such a small value may place in the calculation error. More importantly, when two states have similar total energies, the real state adopted by the material is not determined by the energy any more.^{11–13} For example, Ceder *et al.* found that in r -Li(Co,Al)O₂ the formation enthalpy is small enough (30 meV/f.u.) to allow for the entropy-driven synthesis.¹⁰ Popović *et al.* also reported a mixed AF+F magnetic ground state for NaTiSi₂O₆, although the energy of F state is 90 meV/f.u. lower than that of AF+F state.¹¹

Additionally, for r -LiMnO₂ with HS state, the partially occupied e_g states require JT distortion to eliminate the degeneration and decrease the system's energy until the increase in elastic energy halts the distortion. In order to prove this argument, we have calculated the total energies of m -LiMnO₂ with the same method and settings.¹³ It is found that by the JT distortion, the energy benefit is as large as 175 meV/f.u. for the HS state but only 8 meV/f.u. for the LS state. We also calculated the JT transition temperature as 1910 K and 4 K for the HS and LS states, respectively. This fact implies that for the HS state the JT distortion always exists in the crystalline state, because 1910 K is much higher than the melting point of this system. On the contrary, the JT distortion disappears at the temperature above 4 K in the LS state and thus r -LiMnO₂ can be crystallized.¹³ Therefore, we suggest that r -LiMnO₂ could be synthesized as long as the Mn³⁺ ion is in the LS state. This result is consistent with other theoretical studies.^{4,13,14}

B. Electronic structures and properties of r -LiMnO₂

In order to understand the properties of r -LiMnO₂, and to find out possible synthesizing routes for r -LiMnO₂, it is very effective to investigate its electronic structures. Figure 1 shows the calculated band structures around the Fermi level (E_F , set as 0 eV) for the LS state, the stable state of

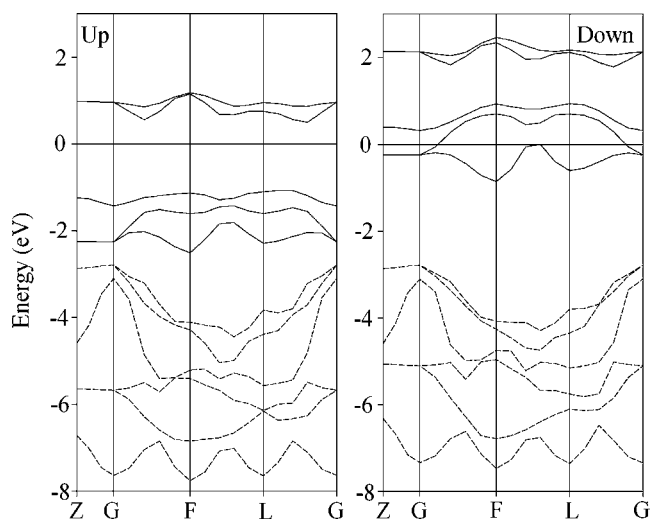


FIG. 1. Band structures of r -LiMnO₂ with LS state. The spin-up/spin-down subbands are plotted in the “Up”/“Down” column.

r -LiMnO₂. Spin-up (\uparrow) and spin-down (\downarrow) subbands are plotted separately in the “Up” (left) and “Down” (right) column, respectively. Each subband contains 11 bands, where the top five mainly originate from the five 3d orbitals of the Mn atom and the bottom six predominantly from the six 2p orbitals of the two O atoms in the primitive cell. These assignments are evident from the corresponding density of states (DOS) presented in Fig. 2. Accordingly, we denote the bottom six levels as O-2p bands (dash lines), which are bonding properties, and the top five levels as Mn-3d bands (solid lines), which are split by the ligand field into upper two antibonding e_g bands and lower three nonbonding t_{2g} bands with a distinct energy gap Δ_o .^{3,13,14} Figure 1 shows that occupied Mn- t_{2g} bands consist of three spin-up and one spin-down levels, which indicates that the Mn ion is indeed in the LS state with an oxidation state of 3+.

With LS Mn³⁺ ion, there are no antibonding e_g electron but only nonbonding t_{2g} electrons in r -LiMnO₂. Thus r -LiMnO₂ is classified as t_{2g} electron system. It is different from most of the other manganites, e_g electron system, in which Mn³⁺ ion is in the HS state. Therefore, r -LiMnO₂ can exhibit new and unique properties.

From Figs. 1 and 2, one can note that the most impressive feature is that there are partially filled $t_{2g}(\downarrow)$ states but not

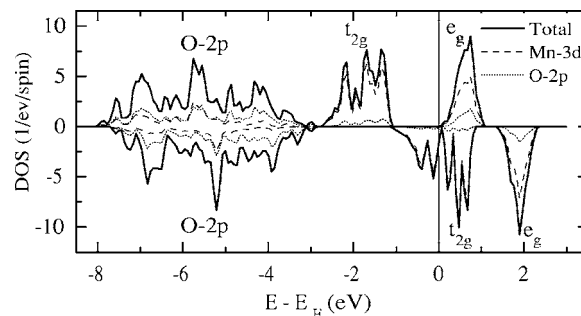


FIG. 2. DOS of r -LiMnO₂ with LS state. In this energy range, the Li-s, Mn-s, Mn-p and O-s contributions are negligible and not shown. Spin-up/spin-down states are plotted along the positive/negative ordinate.

any spin-up states near E_F , which indicates that the spin-down subbands exhibit metallic character and the spin-up ones insulating with an energy gap of 1.567 eV. The insulating gap lies between the $t_{2g}(\uparrow)$ and $e_g(\uparrow)$ states, opened by the ligand field effect. In the metallic spin-down subbands, E_F locates near a minimum in the $t_{2g}(\downarrow)$ DOS (Fig. 2), which reveals the system is stable according to the Stoner criterion.^{9,15} In other work,⁴ E_F locates at the peak of spin-polarized DOS, thus corresponding to an unstable system. We attribute the improvement of our calculation to the full relaxation of the structure. Such a feature in our electronic structures suggests that r - $LiMnO_2$ is a possible half-metal with 100% spin polarization (P), which can be used in the spintronics.¹⁵

Nevertheless, Fig. 1 shows that the $t_{2g}(\downarrow)$ bands are degenerated between Z and Gk points, and this degenerated component consists of flat bands, which corresponds to a large effective mass of the conducting electrons. As a result, although r - $LiMnO_2$ is a possible half-metal with $P=100\%$, its electronic conductivity may be much lower than other typical half-metal, and further theoretical and experimental works need to be carried out for verifying this ‘‘spintronics’’ prediction.

Another distinct character in the electronic structures of r - $LiMnO_2$ is that the Mn-3d and O-2p PDOS overlap heavily in the energy regions of the e_g and O-2p bands, while the t_{2g} bands arise almost only from the Mn-3d PDOS, which reveals that O-2p, t_{2g} , and e_g bands are bonding, non-bonding and antibonding characters, respectively. Because of the presence of other states such as Li-1s, 2s, Mn-4s, 4p, and O-2s (not shown in Fig. 2) and the translational invariance,¹⁶ the nonbonding t_{2g} bands deduced from the simplified diagrams of ionic molecular-orbital theory exhibit some degree of bonding character as revealed by the emergence of weak O-2p states in their energy range. The overlap of Mn-3d and O-2p PDOS between about -8 eV and -3 eV suggests that there is hybridization between them. Because the Mn-3d bands have an exchange splitting (Δ_S) as large as 1.825 eV [taking the midpoints of the $t_{2g}(\uparrow)$ and $t_{2g}(\downarrow)$ manifolds], exchange splitting amounting 0.493 eV is introduced in the O-2p bands by the hybridization between Mn-3d and O-2p states. The heavily hybridized e_g states are all above E_F , making some of the O-2p states empty. Thus, the O ion is actually partially ionized. At the same time, the absence of Li-2s states below E_F reveals that the Li ion is fully ionized. Therefore, in order to keep the electronic neutrality, the Mn ion is partially ionized, i.e., the number of electrons occupied the Mn-3d bands is larger than 4, which answers for the deviation from the normal ionic scenario in the band structures (Fig. 1).

Traditionally, r - $LiMnO_2$ is regarded as a promising cathode material to replace r - $LiCoO_2$ for rechargeable lithium-ion batteries,⁴⁻⁷ which can be ensured by the fully ionized Li ion and hybridization between the Mn and O ions calculated above. First, the fully ionized Li ion combining the layered structure leads to an easy extraction/insertion of Li^+ ions upon the charge/discharge cycling, which ensures a good electrochemical activity of this material. Second, the hybridization between the Mn and O ions makes the electrostatic

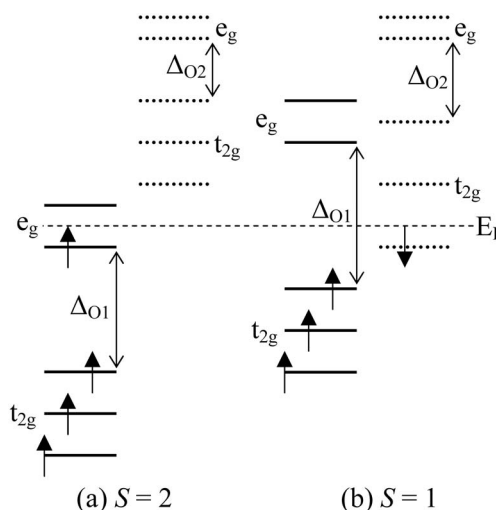


FIG. 3. Schematic illustration of the band structures for (a) HS and (b) LS states, where spin-up/spin-down levels are drawn with solid/dot lines and E_F with dash line. The three t_{2g} levels and the two e_g levels are degenerate, respectively.

repulsion between the O layers much smaller than that expected using formal charges.¹⁷ Therefore, a large fraction of Li^+ ions can be extracted from r - $LiMnO_2$ without destroying the layered structure, which ensures a high reversible capability during the electrochemical cycling. Third, the partially reduced O ions have a potential to function as the electron acceptor upon the Li^+ insertion, which ensures that doping with other M ions, even nontransition metals, can be used to optimize the material but without damage to the electrochemical properties as suggested by Ceder *et al.*¹⁰ Because pure r - $LiMnO_2$ still remains purely an imaginative figment until now, this is especially important to the realization of synthesis of cation-doped r - $LiMnO_2$.

Furthermore, LS Mn^{3+} ion does not have occupied degenerate e_g orbitals, so that it is JT inactive. Consequently, during the charge/discharge process the Mn ion is not cycled between the JT active and inactive valence states, which does not cause a breakup of the material, opposite to what happens in m - $LiMnO_2$.^{4,5} Compared to normally insulating cathodes, such as r - $LiCoO_2$, half-metallic character of r - $LiMnO_2$ induced by LS Mn^{3+} ion can increase the electric conductivity, thereby improving the safety of lithium-ion batteries. As a conclusion, r - $LiMnO_2$ with the LS state seems to exhibit good electrochemical properties based on our first-principles calculations.

Additionally, LS Mn^{3+} ion occupies all three t_{2g} orbitals and leaves all e_g empty (Fig. 3), similar to HS Mn^{4+} ion but different from HS Mn^{3+} ion. Therefore, based on the characters of the electronic structures, it is reasonable to predict that the excitation spectra of Mn ion in r - $LiMnO_2$ will be similar to that of Mn^{4+} ion but not HS Mn^{3+} ion in the typical manganites, such as o - $LiMnO_2$. This finding can explain the contradiction in the experiment on Cr-doped $LiMnO_2$, where the Cr K -edge spectra were identical to that of trivalent $LiCrO_2$ but the Mn K -edge spectra seemed to be much closer to that of tetravalent Li_2MnO_3 than trivalent o - $LiMnO_2$.⁷ A similar explanation can be ap-

plied to explain the conflicts in Co-doped r -LiMnO₂, where Armstrong *et al.* reported that the oxidation state of Co ion is 3+ but Prasad *et al.* found it is 2+ when no Mn⁴⁺ ions were detected.^{4,5}

To sum up, we suggest an unusual LS Mn³⁺ ion in r -LiMnO₂ *via* GGS method. For comparison, LSDA calculations were carried out, too. The LSDA results also show that the LS state is most stable among the three possible spin configurations and the corresponding electronic structures are half-metallic. Nevertheless, for the LS state, the LSDA exchange splitting is not large enough to separate the spin-up and spin-down t_{2g} subbands entirely and the total energies is much higher than that of the GGS solution by 12.944 eV/f.u.. Moreover, LSDA calculations show that the total energy of r -LiMnO₂ is lower than that of m -LiMnO₂, which conflicts with the experiments and implies that the LSDA cannot produce a true ground state in this Mn oxide, in contrast to the GGS.^{10,13} Therefore, it is reasonable to conclude that the GGS is superior to the LSDA in describing the LiMnO₂ system.

C. Proposed approaches for synthesizing r -LiMnO₂

Usually, the Mn³⁺ ion in inorganic compound prefers adopting the HS state and exhibiting the JT distortion, which may answer for the reason why undistorted r -LiMnO₂ is very difficult to synthesize. By comparing the electronic structures of the HS and LS r -LiMnO₂, we gain some useful guidance for its synthesis.

Figure 3 presents the schematic illustration of the band structures for the HS and the LS states. One can find that the most visible change from the HS to the LS state is that the ligand field splitting Δ_0 in both spin subbands is enlarged, which raises the $e_g(\uparrow)$ levels and lowers the $t_{2g}(\downarrow)$ levels, thereby making the former above the latter. It is well known that the Δ_0 depends on the Mn-O bond length (L),^{3,13,18} which is also supported by the change in the L values listed in Table I. For instance, based on the systemic studies on Li_xCo_{1-x}O, van Elp *et al.* have found out experimentally that the Co³⁺ LS ground state in r -LiCoO₂ is stabilized by the strong enough ligand field resulting from the strongly reduced Co-O interatomic distance.¹⁸ Therefore, in order to obtain r -LiMnO₂, one should manage to compress the Mn-O bond, affording a strong enough ligand field to stabilize the LS state. Because the structure of r -LiMnO₂ is constructed by edge-shared regular MnO₆ octahedrons, shortening the Mn-O bond must lead to a decrease in the system's volume (V) (Table I).

According to the principles deduced above, three possible scenarios can be brought forward: (1) High-pressure experiment under low temperature can be an effective method to synthesize r -LiMnO₂, because high pressure can compress the system's volume (and the Mn-O bond) and previous reports have found out that low temperature is of great help to stabilize low-spin state.^{9,19} (2) Thin-film growth with some preferred orientation may provide the mismatching pressure for compressing the Mn-O bond. These two ways are especially suitable to synthesize pure r -LiMnO₂. (3) Doping other cation ions to replace Mn ion. Assuming the doping

follows Vegard's law, only r -LiMO₂ with a shorter M-O bond length than that of pure r -LiMnO₂ can be used to form rhombohedral "solid solution" with r -LiMnO₂. Ceder *et al.* have studied systematically r -LiMO₂ (M =Ti, V, Mn, Co, Ni, Cu, Zn, and Al) with nonmagnetic LDA method.³ From their calculated M-O bond lengths, we find that Co and Ni are the only two candidates whose M-O bond lengths are shorter than Mn-O bond length. For Cr³⁺ ion, its ionic radius (0.61 Å) is smaller than that of HS Mn³⁺ ion (0.645 Å),⁷ but it is larger than that of LS Mn³⁺ ion (0.58 Å).²⁰ Additionally, Cr is to the left of Mn in the Periodic Table and has a smaller electronegativity than Mn atom, so doping with Cr can push the surrounding O atoms towards the nearest Mn atoms, which is similar to what happens when replacing Re by Mo or W in Sr₈CaRe₃Cu₄O₂₄.²¹ Consequently, the Mn-O bond is shortened effectively by both ionic size and electronegativity effect. Therefore, Cr as well as Co and Ni can be used as a dopant to stabilize the rhombohedral symmetry of r -LiMnO₂, which agrees well with the experiments.⁵⁻⁷

D. Experimental proof for LS Mn³⁺ ion

It is well known that transition metal oxides, including Mn-oxides, always are correlated electron systems. For these systems, even though previous reports have suggested that GGS, even LSDA method sometimes are accurate enough to describe the electronic structures,^{3,4,9-21} they are both band pictures and do not take self-interactions into account. As a result, they always underestimate the energy gaps and are incapable of describing the metal-insulator transition of the Mott-Hubbard kind. Therefore, "more proper" correlated electron methods such as LSDA+U (Ref. 22) or self-interaction-corrected (SIC) LSDA (Ref. 23) are necessary for these subjects. For example, when LSDA method describes wrongly m -NaNiO₂ and r -LiNiO₂ as metals, LSDA+U and SIC LSDA approaches respectively open an insulating gap correctly.

Of course, there is a huge difference between r -LiMnO₂ (LS Mn³⁺ ion, $t_{2g}^4 e_g^0$) and NaNiO₂/LiNiO₂ (LS Ni³⁺ ion, $t_{2g}^6 e_g^1$),^{22,23} because the former is t_{2g} electron system and the latter e_g electron systems. In fact, we have reported with the GGS method that m -LiMnO₂ (HS Mn³⁺ ion, $t_{2g}^3 e_g^1$), which belongs to e_g electron system as NaNiO₂/LiNiO₂, is insulating, consistent well with the experiments.¹³ Therefore, it may be uncontradicted that m -NaNiO₂ and r -LiNiO₂ are insulators while the hypothetical r -LiMnO₂ is a possible half-metal. Nevertheless, r -LiMnO₂ is a similar compound to m -NaNiO₂ and r -LiNiO₂, where they have very similar structures and all belong to a correlated electron systems. Even though the GGS includes gradient corrections beyond LSDA, it still has the possibility that the method fails to give the true electronic structures of r -LiMnO₂.

In order to test the validity of our calculations, we choose Cr as the dopant and obtain homogeneous r -Li(Mn,Cr)O₂ solid solutions *via* hydrothermal reaction. We used Cr but not Co or Ni, because LiCrO₂ has an equilibrium isostructure to r -LiMnO₂ and Cr ion has +3 oxidation state in r -Li(Mn,Cr)O₂, but Co and Ni dopants have been found theoretically and experimentally to adopt +2 oxidation

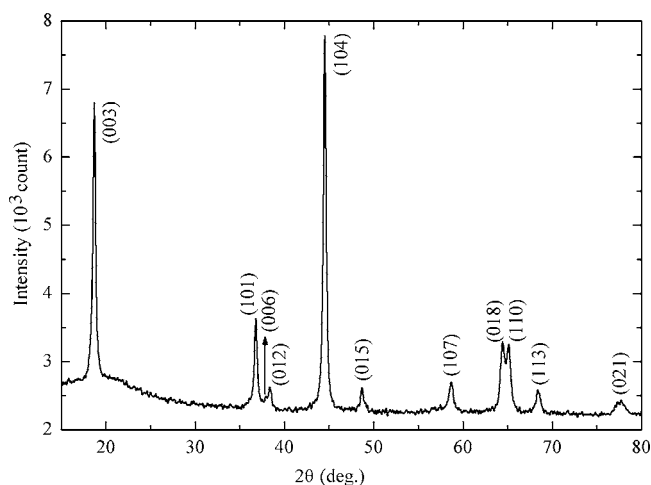


FIG. 4. Powder XRD pattern at room temperature for $r\text{-LiMn}_{0.65}\text{Cr}_{0.35}\text{O}_2$.

state.^{4,7} Therefore, doping with Co or Ni will drive some Mn ions to adopt +4 oxidation states, which will destroy the electronic configuration of Mn ions in $r\text{-LiMnO}_2$ and may induce some uncertain influences.

With Optima 3300 DV inductively coupled plasma spectrometer (ICP, Perkin Elmer Inc.) combined x-ray photoelectron spectroscopy (XPS), the composition of the production was determined to be $\text{LiMn}_{0.65}\text{Cr}_{0.35}\text{O}_2$. The crystal structure of the samples was characterized by powder x-ray diffraction (XRD) at room temperature on a Bruker AXS diffractometer with $\text{Cu } K\alpha_1$ radiation ($\lambda = 1.5406 \text{ \AA}$). The diffraction pattern is represented in Fig. 4. It is found that all the peaks are very sharp and can be indexed based on the $R\bar{3}m$ symmetry, indicating that $r\text{-LiMn}_{0.65}\text{Cr}_{0.35}\text{O}_2$ is crystallized well in a single phase. The clear splitting of the (006, 102) and (108, 110) double-peaks supports again that the material is crystallized in the $\alpha\text{-NaFeO}_2$ structure with $R\bar{3}m$ space group.^{24,25} From least-squares fitting analysis, the lattice parameters and V were calculated and compared with the calculated values (see Table I). The experimental data are much closer to those of the LS state than those of the HS state, which suggests a LS $r\text{-LiMnO}_2$. Additionally, smaller experimental data compared to the calculated ones of the LS state can be noted because of the Cr doping.

In order to test the spin state of the Mn^{3+} ion, we have measured the dc magnetization (M) between 4 and 300 K in a magnetic field (H) of 100 Oe. M was measured after field cooling (FC) and zero-field cooling (ZFC), respectively with a superconducting quantum interference device (SQUID) in the magnetic property measurement system (MPMS-XL, Quantum Design Co.). The results are shown in Fig. 5. The inverse susceptibility is plotted in Fig. 6, including a Curie-Weiss law²⁶ $\chi = \frac{C}{T - \Theta}$ (solid line) fitting to the high-temperature data above 150 K, where χ is the susceptibility M/H , T is the absolute temperature, C is the Curie constant and Θ is the Weiss constant.

From Fig. 6, C constant is fitted to be 0.0147 emu K/g Oe, with which the effective moment $\mu_{\text{eff}} = 3.313 \mu_B/\text{f.u.}$ is obtained by evaluating the relation²⁷ $C = \frac{N\mu_{\text{eff}}^2}{3k_B}$, where N is the

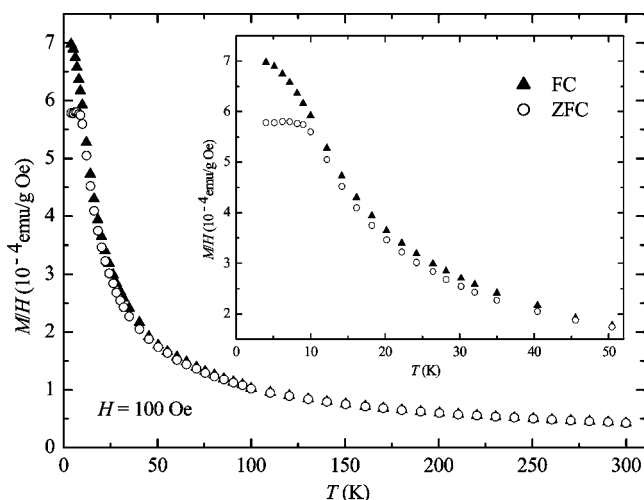


FIG. 5. Field-cooled (FC) and zero-field-cooled (ZFC) dc magnetization (M) in a magnetic field (H) of 100 Oe as a function of temperature (T) between 4 and 300 K.

number density of magnetic ions (i.e., Mn and Cr in the present work) per unit gram, k_B is the Boltzmann's constant. Since previous experimental⁷ and theoretical⁴ studies have proved that the Cr dopant in $r\text{-LiMnO}_2$ adopts an oxidation state of 3+ with the HS state ($S = 3/2$), $\mu_{\text{eff-Cr}} = 3.873 \mu_B$ is calculated from the equation²⁷ $\mu_{\text{eff}} = 2\sqrt{S(S+1)}$ by assuming that μ_{eff} depends only on S . Combining equation $\mu_{\text{eff}} = \sqrt{0.65\mu_{\text{eff-Mn}}^2 + 0.35\mu_{\text{eff-Cr}}^2}$, $\mu_{\text{eff-Mn}} = 2.97 \mu_B$, and $S = 1.07$ are calculated for the Mn ion in the sample, which are very close to our theoretically expected value $S = 1.00$ for the LS Mn^{3+} ion but far from $S = 1.90$ for the HS Mn^{3+} ion (Table I). Therefore, the Mn^{3+} ions in $r\text{-LiMn}_{0.65}\text{Cr}_{0.35}\text{O}_2$ adopt the LS states indeed, proving our theoretical result. The deviation from 1.00 can be partially ascribed to the possible contribution of orbital moment, which is not considered in the spin-only scenario.

Besides, it is necessary to discuss briefly the magnetic properties of $r\text{-LiMn}_{0.65}\text{Cr}_{0.35}\text{O}_2$. In Fig. 5, it can be noted

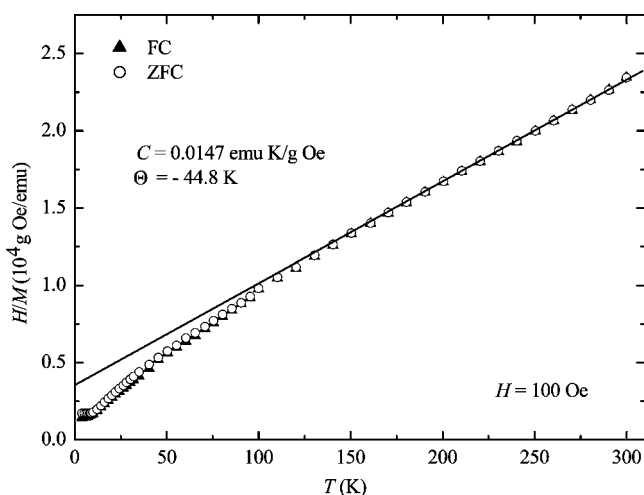


FIG. 6. Inverse FC and ZFC dc magnetization (M) in a magnetic field (H) of 100 Oe as a function of T between 4 and 300 K.

that the main striking features include: (1) the abrupt increase below about 50 K, which indicates the existence of a large dominant ferromagnetic (FM) component;^{26–28} (2) the absolute FC, ZFC divergence below about 10 K, which belongs to the common feature of all kinds of magnetic systems showing magnetic hysteresis behavior and it is possibly due to a FM, ferrimagnetic (FiM), canted anti-FM (CAF) or spin-glass (SG) transition;^{26–28} (3) the approach to saturation below 5 K and the absence of sharp maximum in the ZFC branch, opposite to usual AF or SG states.^{26–28} For the negative value of $\Theta = -44.8$ K deduced from Fig. 6, it reveals that weak AF interaction are dominant over FM interaction in the paramagnetic (PM) T regime. Nevertheless, a small negative/positive value of Θ cannot determine that the material has AF/FM ground state at low T . For instance, CeAgSb_2 single crystal below 9.8 K is FM order along c axis with $\Theta = -63.9$ K and is AF order perpendicular to c axis with $\Theta = 5.05$ K.²⁹ It is also found $\Theta = 18.3$ K and $\Theta = 20.8$ K, respectively, for the AF EuCu_2As_2 (Ref. 30) and $\text{SrFeO}_{2.83}$,³¹ while for high- T FM SnO_2 with slight Fe doping, its Θ values are negative.³² Obviously, the magnetic properties of the synthesized $r\text{-LiMn}_{0.65}\text{Cr}_{0.35}\text{O}_2$ are very complex and unique, which may be caused by the Cr-doping, or by the nature of $r\text{-LiMnO}_2$.

In summary, the synthesis of Cr-doped $r\text{-LiMnO}_2$ and the results of magnetic measurements reveal that the main GGS result of the present work is correct: the Mn^{3+} ion in $r\text{-LiMnO}_2$ is truly in the unusual low-spin state. Nevertheless, we suggest that a more localized scenario, such as LSDA+U, SIC LSDA, and other correlated electron methods, should be employed to verify the possibility of the this

material's half-metallicity. In order to clarify the electronic and magnetic properties of $r\text{-LiMnO}_2$, more detailed experimental and theoretical studies are necessary to be carried out.

IV. CONCLUSIONS

First-principles calculations with GGS method have been employed to investigate the electronic structures of hypothetical $r\text{-LiMnO}_2$. It is predicted that $r\text{-LiMnO}_2$ has an unusual spin state with LS Mn^{3+} ion ($S=1$), which makes this material not only a good cathode material for rechargeable lithium-ion battery, but also a possible half-metal for spintronics. Based on the theoretical analysis, we suggest that the synthesis of $r\text{-LiMnO}_2$ can be realized by managing to compress the Mn-O bond length, such as by high-pressure experiment under low temperature, thin-film growth with preferred orientation or doping with other transition-metal ions such as Co, Ni, or Cr. Following the proposed approaches, we have successfully obtained well crystallized $r\text{-LiMn}_{0.65}\text{Cr}_{0.35}\text{O}_2$ through hydrothermal reaction. Furthermore, we have carried out SQUID magnetic measurements on the sample and found out the LS Mn^{3+} configuration, which confirms the theoretical finding.

ACKNOWLEDGMENTS

This work was sponsored by both the Special Funds for Major State Basic research Project of China under Grant No. 2002CB211802 and a component part of Key Project 10411 from the Ministry of Education, China.

*Corresponding author. Email address: gchen@jlu.edu.cn

¹A. R. Armstrong and P. G. Bruce, *Nature (London)* **381**, 499 (1996).

²F. Capitaine, P. Gravereau, and C. Delmas, *Solid State Ionics* **89**, 197 (1996).

³M. K. Aydinol, A. F. Kohan, G. Ceder, K. Cho, and J. Joannopoulos, *Phys. Rev. B* **56**, 1354 (1997).

⁴R. Prasad, R. Benedek, A. J. Kropf, C. S. Johnson, A. D. Robertson, P. G. Bruce, and M. M. Thackeray, *Phys. Rev. B* **68**, 012101 (2003). R. Prasad, R. Benedek, A. J. Kropf, C. S. Johnson, A. D. Robertson, P. G. Bruce, and M. M. Thackeray, *ibid.* **71**, 134111 (2005).

⁵A. R. Armstrong, A. D. Robertson, R. Gitzendanner, and P. G. Bruce, *J. Solid State Chem.* **145**, 549 (1999).

⁶T. Ohzuku and Y. Makimura, *Chem. Lett.* **8**, 744 (2001).

⁷S. T. Myung, S. Komaba, N. Hirotsaki, N. Kumagai, K. Arai, R. Kodama, and I. Nakai, *J. Electrochem. Soc.* **150**, A1560 (2003).

⁸Accelrys Inc., CASTEP Users Guide, San Diego: Accelrys Inc. (2001); V. Milman, B. Winkler, J. A. White, C. J. Pickard, M. C. Payne, E. V. Akhmatkaya, and R. H. Nobes, *Int. J. Quantum Chem.* **77**, 895 (2000).

⁹I. Solovyev, N. Hamada, and K. Terakura, *Phys. Rev. B* **53**, 7158 (1996); J. Hafner and D. Hobbs, *ibid.* **68**, 014408 (2003).

¹⁰S. K. Mishra and G. Ceder, *Phys. Rev. B* **59**, 6120 (1999).

¹¹G. Ceder, Y. -M. Chiang, D. R. Sadoway, M. K. Aydinol, Y.-I.

Jang, and B. Huang, *Nature (London)* **392**, 694 (1998).

¹²Z. S. Popović, Z. V. Sljivancanin, and F. P. Vukajlovic, *Phys. Rev. Lett.* **93**, 036401 (2004).

¹³Z.-F. Huang, X. Meng, C.-Z. Wang, Y. Sun, and G. Chen, *J. Power Sources* **158**, 1394 (2006).

¹⁴T. Amriou, B. Khelifa, H. Aourag, S. M. Aouadi, and C. Mathieu, *Chem. Phys.* **92**, 499 (2005).

¹⁵S. P. Lewis, P. B. Allen, and T. Sasaki, *Phys. Rev. B* **55**, 10253 (1997).

¹⁶M. T. Czyzyk, R. Potze, and G. A. Sawatzky, *Phys. Rev. B* **46**, 3729 (1992).

¹⁷Y. Koyama, Y.-S. Kim, I. Tanaka, and H. Adachi, *Jpn. J. Appl. Phys., Part 1* **38**, 2024 (1999).

¹⁸J. van Elp, J. L. Wieland, H. Eskes, P. Kuiper, G. A. Sawatzky, F. M. F. de Groot, and T. S. Turner, *Phys. Rev. B* **44**, 6090 (1991).

¹⁹M. Abbate, J. C. Fuggle, A. Fujimori, L. H. Tjeng, C. T. Chen, R. Potze, G. A. Sawatzky, H. Eisaki, and S. Uchida, *Phys. Rev. B* **47**, 16124 (1993).

²⁰Y. Koyama, Y. Makimura, I. Tanaka, H. Adachi, and T. Ohzuku, *J. Electrochem. Soc.* **151**, A1499 (2004).

²¹X. Wan, M. Kohno, and X. Hu, *Phys. Rev. Lett.* **95**, 146602 (2005).

²²H. Meskine and S. Satpathy, *J. Appl. Phys.* **97**, 10A314 (2005).

²³L. Petit, G. M. Stocks, T. Egami, Z. Szotek, and W. M. Temmerman, *Phys. Rev. Lett.* **97**, 146405 (2006).

- ²⁴Z.-F. Huang, Y.-J. Wei, W. Liu, X.-G. Xu, C.-Z. Wang, and X. Meng, G. Chen, Chem. J. Chinese Univ. **25**, 810 (2004).
- ²⁵Y. S. Meng, Y. W. Wu, B. J. Hwang, Y. Li, and G. Ceder, J. Electrochem. Soc. **151**, A1134 (2004).
- ²⁶Y.-I. Jang, F. C. Chou, and Y.-M. Chiang, Appl. Phys. Lett. **74**, 2504 (1999).
- ²⁷J. Sugiyama, H. Nozaki, J. H. Brewer, E. J. Ansaldo, G. D. Morris, and C. Delmas, Phys. Rev. B **72**, 144424 (2005).
- ²⁸M. Pissas and G. Papavassiliou, J. Phys.: Condens. Matter **16**, 6527 (2004).
- ²⁹E. Jobiliong, J. S. Brooks, E. S. Choi, H. Lee, and Z. Fisk, Phys. Rev. B **72**, 104428 (2005).
- ³⁰K. Sengupta, P. L. Paulose, E. V. Sampathkumaran, Th. Doert, and J. P. F. Jematio, Phys. Rev. B **72**, 184424 (2005).
- ³¹S. Srinath, M. M. Kumar, M. L. Post, and H. Srikanth, Phys. Rev. B **72**, 054425 (2005).
- ³²A. Punnoose, J. Hays, A. Thurber, M. H. Engelhard, R. K. Kukkadapu, C. Wang, V. Shutthanandan, and S. Thevuthasan, Phys. Rev. B **72**, 054402 (2005).